Journal of **N**onlinear **A**nalysis and **O**ptimization
Vol. 15, Issue. 1, No.3 : 2024
ISSN : **1906-9685**

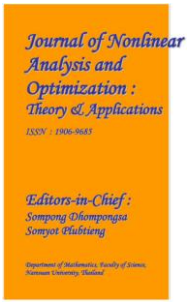

PREPARATION AND CHARACTERIZATION OF DIARUN DOPED MAGNESIUM OXIDE NANOCOMPOSITES: A WET CHEMICAL APPROACH

M.UDAYENDIRAN. Research scholar, PG & Research Department of Physics, Periyar Arts College, Cuddalore, Tamil Nadu, India
Dr. A. CHRISTY FERDINAND PG & Research Department of Physics, Periyar Arts College, Cuddalore, Tamil Nadu, India Email: christyferdinand2@gmail.com
T. KASTHURY PG & Research Department of Physics, Periyar Arts College, Cuddalore, Tamil Nadu, India.

Abstract

Diarun 50% + MgO 50% nanocomposites were synthesized via wet chemical methods and subsequently annealed at temperatures of 200°C, 400°C, and 600°C. The annealing process was employed to enhance the crystallinity and interfacial interactions between the constituents, thereby improving the overall thermal stability and performance of the nanocomposites. A comprehensive characterization was conducted using X-ray diffraction (XRD), Fourier-transform infrared spectroscopy (FTIR), ultraviolet-visible spectroscopy (UV), scanning electron microscopy (SEM), atomic force microscopy (AFM), and particle size analysis. XRD analysis revealed the crystalline structure evolution, while FTIR provided insights into chemical bonding. UV spectroscopy elucidated the optical properties, while SEM and AFM offered surface morphology and topography details. Particle size analysis enabled the determination of size distribution. This multi-technique approach provides a thorough understanding of the structural, chemical, optical, morphological, and size-related properties of Diarun 50% + MgO 50% nanocomposites, crucial for their potential applications.

Keywords:
Diarun, Magnesium Oxide, Wet chemical synthesis, XRD, SEM.

1. Introduction

Nanoparticles have gained significant attention in various scientific fields due to their unique properties and potential applications in diverse areas, including medicine, electronics, and catalysis [1]. Among the myriad nanoparticles explored, magnesium oxide (MgO) nanoparticles exhibit exceptional properties such as high surface area, chemical stability, and biocompatibility, making them promising candidates for multifaceted applications [2-4].

Diarun, a herbal extract derived from Rumi Herbals India, has emerged as a promising dopant for modifying the properties of metal oxide nanoparticles. With its rich composition of organic compounds and bioactive constituents, Diarun offers a novel approach to enhance the functionality and performance of nanomaterials [5].Diarun is a pharmaceutical compound that has garnered considerable attention in recent years due to its potential therapeutic applications in the field of medicine. This drug, with its unique chemical composition and pharmacological properties, holds promise for addressing various medical conditions and improving patient outcomes.

Synthesis methods play a crucial role in tailoring the size, morphology, and surface properties of MgO nanoparticles [6,7], thereby influencing their performance and applicability [8]. Various synthesis techniques including sol-gel [9], hydrothermal [10], combustion [11], and wet chemical [12] methods have been employed to fabricate MgO nanoparticles with controlled characteristics. Moreover, the dopant-induced modification of MgO nanoparticles has emerged as an effective strategy to further enhance their properties for specific applications [13]. Doping MgO with different elements

or compounds can introduce new functionalities, improve stability, and enhance performance, thereby expanding the potential applications of MgO nanoparticles [14-16].

In this study, we aim to systematically explore the impact of annealing temperature on the structural, optical, and morphological attributes of Diarun-MgO nanocomposites synthesized through the chemical precipitation method [3,17-26]. Employing a multi dimensional characterization approach encompassing X-ray diffraction (XRD), Fourier-transform infrared (FTIR) spectroscopy, UV-Vis spectroscopy, scanning electron microscopy (SEM), atomic force microscopy (AFM), and particle size analysis (PSA), our research endeavours to unravel the structural evolution, phase transitions, chemical bonding, optical properties, surface morphology, and particle size distribution of the nanocomposites across varying annealing temperatures.

This study focuses on the wet chemical synthesis of Diarun-doped MgO nanoparticles and the comprehensive characterization of their physicochemical properties. Diarun belongs to a class of compounds known for their targeted effects on specific biological pathways, making them valuable candidates for the development of novel pharmaceutical interventions. The exploration of Diarun as a therapeutic agent involves understanding its mechanisms of action, pharmacokinetics, and potential applications across a range of medical scenarios.

2. Materials and Methods

2.1. Materials used The materials used in the synthesis include Diarun, procured from Rumi Herbals India. Furthermore, analytical-grade double-distilled water, sodium hydroxide (NaOH), and magnesium oxide (MgO) were employed in the synthesis procedure.

2.2. Synthesis procedure The wet chemical synthesis procedure commenced with the dissolution of 20 grams of Diarun powder in de-ionized water, followed by stirring for 15 minutes at room temperature using a magnetic stirrer. Simultaneously, 20 grams of Magnesium oxide (MgO) were dispersed in double-distilled water. In parallel, a NaOH solution was gradually added drop wise to the Diarun solution until the pH attained 11, and continuous stirring persisted for 30 minutes to facilitate the wet chemical reaction. Throughout this process, the solution exhibited a distinctive dark red colour indicative of the reaction progress. Upon precipitation, the solution underwent intense stirring for an additional 3 hours at 70º C utilizing a hot plate magnetic stirrer. After the wet chemical synthesis phase, the solution underwent thorough washing with hot water (3-5 times) to eliminate impurities. The resultant mixture was then subjected to filtration, and the filtered samples were dried at 70º C for 12 hours to achieve a powdered state. Finally, the synthesized samples underwent annealing at temperatures of 200º C, 400º C, and 600º C, each for duration of 2 hours, aimed at further enhancing their properties.

2.3. Characterisation techniques X-ray diffraction (XRD) patterns were collected for the prepared samples using the powder XRD technique, employing Cu-Kα radiation (λ=1.54060 Å) at 40 KV and 30 mA. Fourier Transform Infrared (FTIR) spectra spanning the range of 4000-400 cm^{-1} were recorded using a Magna IR spectrometer 550 Nicolet UV-visible spectra were captured using the Jasco Nicolet 670 W Japan spectrophotometer. Scanning electron microscopy was employed to examine the morphological characteristics of both pure and variously Diarun doped MgO nanoparticles. Atomic Force Microscopy (AFM) images were obtained using Agilent 5100, USA. The Particle Size Analyzer (Nano Plus Micromeritics) was utilized to analyze the particle size distribution.

3. Results and Discussion

3.1. X-ray Diffraction X-ray diffraction (XRD) analysis was employed to explore the crystalline structure and average crystallite sizes of Diarun 50% + MgO 50% nanocomposites synthesized via wet chemical method. The nanocomposites were subsequently annealed at different temperatures. The XRD patterns obtained at 200°C, 400°C, and 600°C exhibited clear diffraction peaks corresponding to distinct crystallographic planes. The determination of average crystallite sizes was carried out utilizing the Debye's-Scherrer equation ,

$$D = \frac{K\lambda}{\beta COS\theta} \qquad (1)$$

At 200°C, the average crystallite size recorded in Table 1 was 27.91 nm. Subsequent annealing at 400°C led to an increase in the average crystallite size to 21.97 nm, while further annealing at 600°C

resulted in a slightly smaller average crystallite size of 22.07 nm. These results indicate a temperature-dependent influence on crystallite growth within the nanocomposite structure, suggesting that variations in the annealing process impact the material's crystallinity and structural properties. The XRD analysis offers valuable insights into the structural evolution of Diarun-MgO nanocomposites under different annealing conditions.

Additionally, the dislocation density (δ) of Diarun 50% + MgO 50% nanocomposites was investigated at various annealing temperatures. The dislocation density (δ) is calculated using Williamson and small man's formula in lines/m^2

$$\delta = \frac{n}{D^2} \qquad (2)$$

Where n is approximately equal to 1, D is the crystallite size. Results revealed a dislocation density of 1.283×10^{15} lines /m^2 at 200°C, 2.07×10^{15} lines /m^2 at 400°C, and 2.8362×10^{15} lines /m^2 at 600°C. These observations underscore a temperature-dependent influence on dislocation density within the nanocomposite structure, implying that alterations in the annealing process impact the material's structural characteristics.

Williamson-Hall Method In XRD data, the broadening (β_r) of the peaks is due to the combine effect of crystalline size (β_D) and micro strain (β_ε), i.e,
Total broadening = Broadening due to crystallite size + Broadening due to strain

Where β_r is the broadening, β_D is broadening due to crystallite size and β_ε is the broadening due to strain.
From the Scherer equation, we know that,

$$\beta_D = \frac{k\lambda}{D\ Cos\theta} \qquad (4)$$

Where β_D is the FWHM (i.e. broadening of the peak) in radiand, $k = 0.9$ is the shape factor, $\lambda = 0.15406\ nm$ is the wavelength of X-ray source, D is the crystallite size and θ is the peak position in radians.
Similarly, the XRD peak broadening due to micro strain is given by,

$$\beta_\varepsilon = 4\varepsilon\ tan\theta \qquad (5)$$

Where, β_ε is the broadening due to strain, ε is the strain and θ is the peak position in radians.
Putting equation (4) and (5) in equation (3), we get,

$$\beta_r = \beta_D + \beta_\varepsilon \qquad (3)$$

$$\beta_r = \frac{k\lambda}{D\ Cos\theta} + 4\varepsilon\ tan\theta \qquad (6)$$

Therefore, equation (6) can be written as,

$$\beta_r \cos\theta = \varepsilon(4\sin\theta) + \frac{k\lambda}{D} \qquad (7)$$

Equation (7) depicts a linear relationship, where ε signifies the gradient (slope) of the line, and $\frac{k\lambda}{D}$ denotes the y-intercept.
Let's consider the standard equation of a straight line,

$$y = mx + c \qquad (8)$$

Where m is the slope of line and c is the y-intercept.
Comparing equation (7) with equation (8), we have,

$$y = \beta_r \cos\theta \qquad \text{(i)}$$
$$m = \varepsilon \qquad \text{(ii)}$$
$$x = 4\sin\theta \qquad \text{(iii)}$$
$$c = \frac{k\lambda}{D} \qquad \text{(iv)}$$

The value of "m" representing the gradient (slope) of the line, is indicative of the strain "ε". Subsequently, the crystallite size can be calculated from the y-intercept using the formula $\frac{k\lambda}{D}$.

The crystalline size of Diarun 50% + MgO 50% nanocomposites annealed at various temperatures was determined using the Williamson-Hall method. Analysis revealed crystalline sizes of 24.41 nm at 200°C, 26.76 nm at 400°C, and 9.01 nm at 600°C, indicating a temperature-dependent effect on the nanocomposite structure. The slope obtained from the Williamson-Hall plot was 3.856E-4 at 200°C, 0.00152 at 400°C, and 0.00337 at 600°C, corresponding to strains within the

nanocomposites. These findings suggest that variations in the annealing process influence the material's structural characteristics.

Table 1: XRD Analysis of Diarun 50% + MgO 50% Nanocomposites annealed at 200°C, 400°C, and 600°C

Annealing Temperature	Pos. [°2Th.]	FWHM Left [°2Th.]	d-spacing [Å]	Crystallite size D (nm)
200°C	18.4449	0.3936	4.81030	20.45808
	32.8172	0.4723	2.72912	17.54273
	37.9586	0.1574	2.37046	53.39756
	50.8064	0.3936	1.79712	22.35303
	58.6767	0.1968	1.57345	46.32326
	62.0401	0.7872	1.49598	11.77997
	68.3145	0.4723	1.37308	20.33295
	72.0730	0.3936	1.31045	24.9668
400°C	18.5824	0.3936	4.77503	20.46208
	32.9703	0.4723	2.71680	17.54964
	38.0791	0.4330	2.36324	19.41759
	42.4792	0.5510	2.12808	15.47539
	50.8950	0.4723	1.79419	18.63515
	56.7916	0.2755	1.62112	32.79203
	58.7105	0.1968	1.57263	46.33093
	62.0167	0.3936	1.49649	23.55706
	68.4183	1.2595	1.37125	7.629342
	72.2502	0.5510	1.30767	17.85481
600°C	10.7076	1.8893	8.26252	4.225432
	18.6122	0.6298	4.76745	12.78853
	32.5858	0.2362	2.74797	35.05728
	34.4090	0.2362	2.60643	35.22537
	37.8958	0.3936	2.37424	21.34958
	42.8616	0.1968	2.10998	43.38441
	50.7715	0.6298	1.79827	13.96774
	53.7837	0.3936	1.70445	22.63967
	58.6303	0.3936	1.57458	23.15637
	62.0828	0.1968	1.49506	47.13044
	69.0264	1.2595	1.36065	7.657041
	72.2298	0.9446	1.30799	10.41364
	74.3962	0.9446	1.27518	10.56102
	78.3988	0.4723	1.21980	21.71002

Table 2: W-H plot of Diarun 50% + MgO 50% Nanocomposites annealed at 200°C, 400°C, and 600°C

Annealing Temperature	2θ (degree)	2θ in radians	FWHM (β_r) in degree	FWHM in radians	$\beta_r \cos\theta$	$4 \sin\theta$
200°C	**18.4449**	0.160962	**0.3936**	0.00687	0.006781	0.641072
	32.8172	0.286384	0.4723	0.008243	0.007907	1.129942
	37.9586	0.331251	0.1574	0.002747	0.002598	1.300906
	50.8064	0.443369	0.3936	0.00687	0.006205	1.715942
	58.6767	0.512051	0.1968	0.003435	0.002994	1.959864
	62.0401	0.541402	0.7872	0.013739	0.011774	2.061352
	68.3145	0.596156	0.4723	0.008243	0.006821	2.245864

	72.073	0.628956	0.3936	0.00687	0.005555	2.353202
400°C	18.5824	0.162162	0.3936	0.00687	0.006779	0.645809
	32.9703	0.28772	0.4723	0.008243	0.007904	1.135067
	38.0791	0.332303	0.433	0.007557	0.007144	1.304883
	42.4792	0.370701	0.551	0.009617	0.008964	1.449075
	50.895	0.444143	0.4723	0.008243	0.007443	1.718736
	56.7916	0.4956	0.2755	0.004808	0.00423	1.902239
	58.7105	0.512346	0.1968	0.003435	0.002994	1.960893
	62.0167	0.541198	0.3936	0.00687	0.005888	2.060652
	68.4183	0.597062	1.2595	0.021982	0.018179	2.248862
	72.2502	0.630502	0.551	0.009617	0.007768	2.358201
600°C	10.7076	0.093441	1.8893	0.032975	0.032831	0.373222
	18.6122	0.162422	0.6298	0.010992	0.010847	0.646836
	32.5858	0.284365	0.2362	0.004122	0.003957	1.122191
	34.409	0.300275	0.2362	0.004122	0.003938	1.183132
	37.8958	0.330703	0.3936	0.00687	0.006497	1.298833
	42.8616	0.374038	0.1968	0.003435	0.003197	1.461509
	50.7715	0.443065	0.6298	0.010992	0.009931	1.714842
	53.7837	0.469351	0.3936	0.00687	0.006127	1.809231
	58.6303	0.511646	0.3936	0.00687	0.00599	1.958452
	62.0828	0.541775	0.1968	0.003435	0.002943	2.062629
	69.0264	0.602369	1.2595	0.021982	0.018113	2.266384
	72.2298	0.630324	0.9446	0.016486	0.013318	2.357626
	74.3962	0.649229	0.9446	0.016486	0.013132	2.418291
	78.3988	0.684159	0.4723	0.008243	0.006388	2.528085

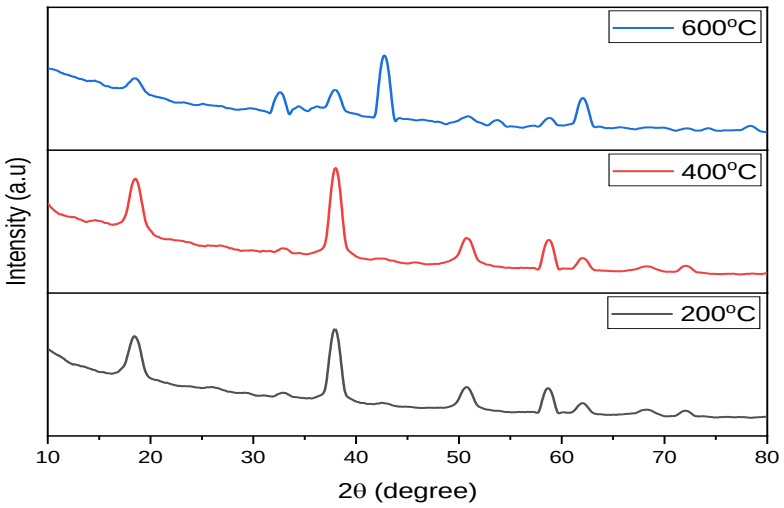

Figure 1: XRD pattern of Diarun50% + MgO 50% Nanocomposites annealed at 200°C, 400°C, and 600°C

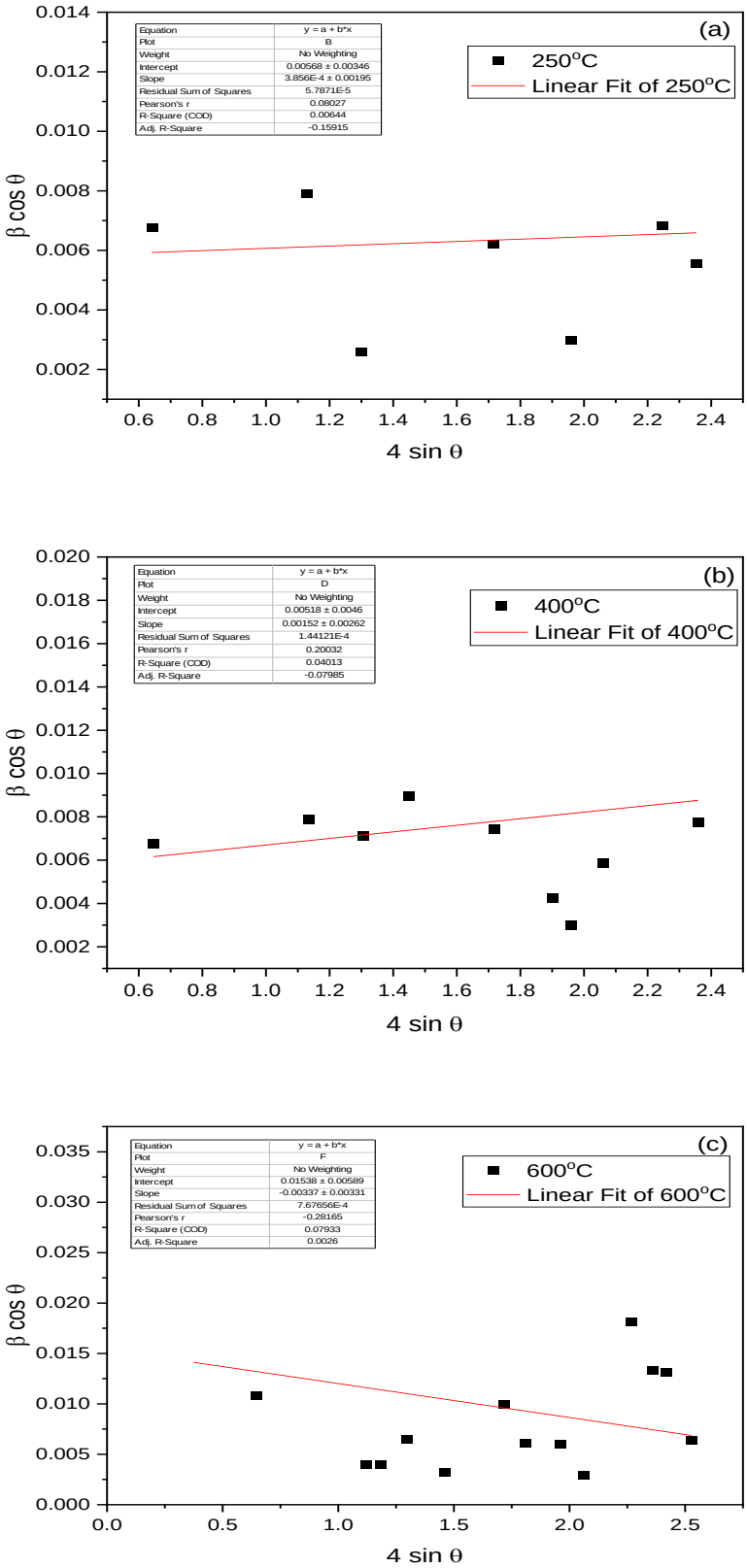

Figure 2: W-H plot of Diarun 50% + MgO 50% Nanocomposites annealed at 200°C, 400°C, and 600°C

3.2. Fourier Transform Infrared Analysis

The FTIR analysis of Diarun 50% + MgO 50% Nanocomposites annealed at different temperatures revealed distinct absorption peaks indicative of specific functional groups within the nanocomposites. At 200°C, prominent peaks were observed at 428.52 cm^{-1} (Mg-O stretching), 451.23 cm^{-1} (Mg-O bending), 466.65 cm^{-1} 532.52 cm^{-1} (Mg-O bending), 1052.07 cm^{-1}, 1325.43 cm^{-1}, 1466.86 cm^{-1},changes in the aromatic and aliphatic C-H stretching vibrations, 3422.27 cm^{-1} and 3698.41 cm^{-1}

(O-H stretching). Upon annealing at 400°C, additional peaks emerged at 419-480 cm^{-1}may be attributed metal oxygen bond and C-O stretching, 516.77 $cm^{-1}$and 571.45 cm^{-1}represent bending vibrations involving Mg-O bonds, and 3698.60 cm^{-1} (O-H stretching). At 600°C, the spectrum exhibited peaks at 425 cm^{-1}, 433.79 cm^{-1}, 442.96 cm^{-1}, 451.85 cm^{-1}, 458.50 cm^{-1}, 463.21 cm^{-1}, 470.35 cm^{-1}, 475.85 cm^{-1}, indicates the various functional groups such as C-O stretching and metal-oxygen bonds, 1469.94 cm^{-1}, 3411.81 cm^{-1}, and 3699.18 cm^{-1} (O-H stretching). These results suggest variations in the chemical composition and bonding within the nanocomposites as a function of annealing temperature.

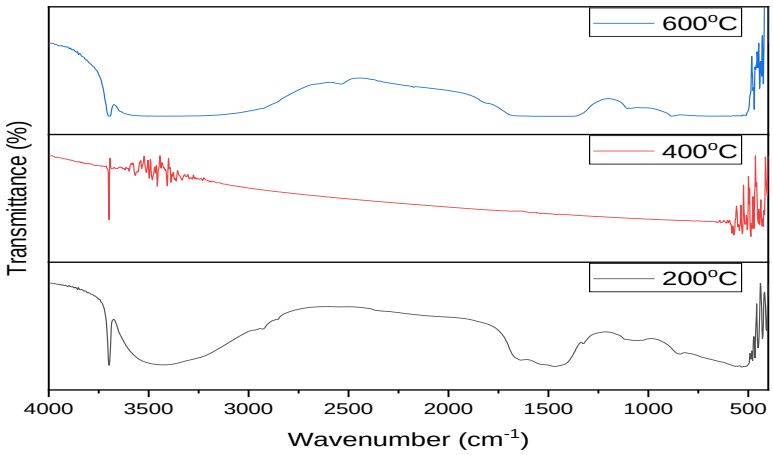

Figure 3: FTIR analysis of Diarun 50% + MgO 50% Nanocomposites annealed at 200°C, 400°C, and 600°C

3.3. Ultraviolet Analysis

The UV absorption spectra of the Diarun 50% + MgO 50% nanocomposites exhibited distinctive absorption peaks corresponding to different annealing temperatures, as illustrated in Figure 4. These absorption peaks represent the absorption of UV light by the nanocomposites, indicating electronic transitions within the material. Furthermore, the bandgap values of the nanocomposites were determined based on the onset of absorption in the UV spectra. This was achieved through Tauc plot analysis, as depicted in Figure 5.

At 200°C annealing temperature, the UV absorption peak was observed at 301 nm. Concurrently, the bandgap value of the nanocomposites was calculated to be 2.76 eV. This absorption peak corresponds to the absorption of UV light by the nanocomposites, signifying electronic transitions within the material. The calculated bandgap value indicates the energy difference between the valence band and the conduction band, providing insights into the nanocomposite's electronic properties. Upon annealing at 400°C, the UV absorption peak shifted to 300 nm, accompanied by a decrease in the bandgap value to 2.67 eV. The shift in absorption wavelength suggests modifications in the electronic structure or composition of the nanocomposites due to annealing at higher temperatures. The decrease in bandgap value indicates a narrowing of the bandgap energy, possibly resulting from enhanced crystallization or phase transformations induced by the annealing process. At 600°C, the UV absorption peak further shifted to 298 nm, accompanied by a reduction in the bandgap value to 2.55 eV. This shift in absorption wavelength and decrease in bandgap value indicate additional alterations in the electronic structure or composition of the nanocomposites at elevated temperatures. The observed changes in the bandgap energy suggest further modifications in the nanocomposites' electronic transitions and energy levels due to annealing-induced structural rearrangements or phase transitions.

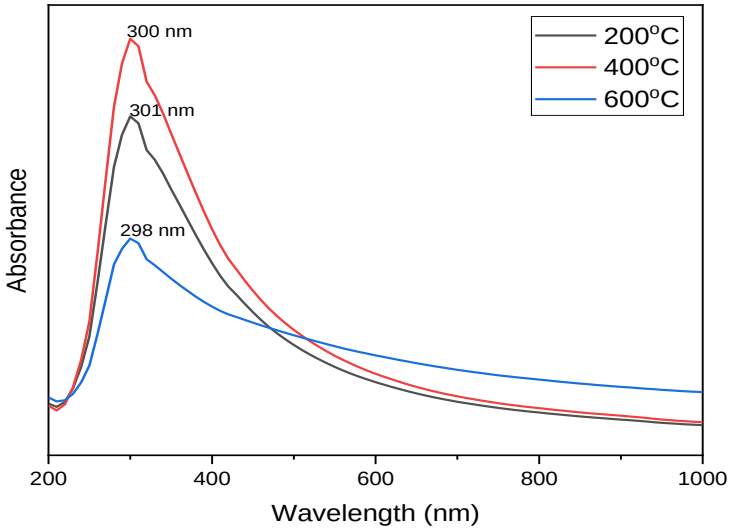

Figure 4: UV analysis of Diarun 50% + MgO 50% Nanocomposites annealed at 200°C, 400°C, and 600°C

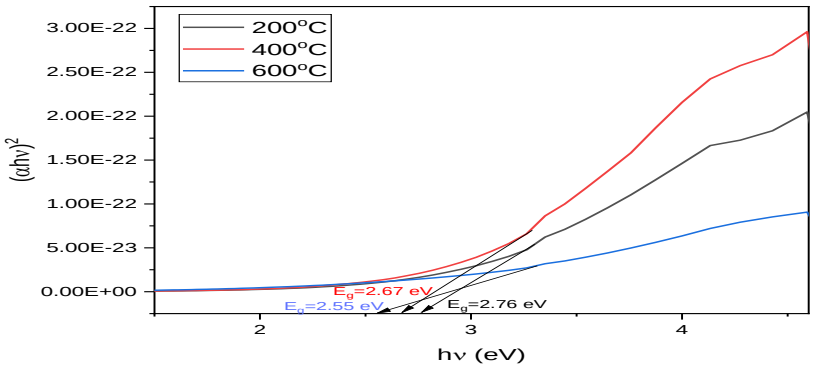

Figure 5: Tauc plot of Diarun 50% + MgO 50% Nanocomposites annealed at 200°C, 400°C, and 600°C

3.4. Scanning Electron Microscope Analysis

SEM micrographs were obtained to investigate the surface morphology of Diarun 50% + MgO 50% nanosamples annealed at different temperatures (200°C, 400°C, and 600°C) by wet chemical synthesis. At 200°C annealing temperature, the SEM micrograph (Figure 6a) revealed nanosamples exhibiting a triticum shape morphology. The particles appeared well-defined with sharp edges, and the average particle size was measured to be approximately 20 nm. The triticum shape morphology suggests a distinctive crystalline structure, which may be attributed to the annealing process at this temperature. Upon annealing at 400°C, the SEM micrograph (Figure 6b) depicted nanosamples with an agglomerated spherical shape morphology. The particles exhibited a tendency to cluster together, forming larger agglomerates compared to the 200°C annealed samples. Despite the agglomeration, the particles maintained a relatively spherical shape. The average particle size was determined to be around 21 nm, slightly larger than that observed at 200°C. At an annealing temperature of 600°C, the SEM micrograph (Figure 6c) exhibited nanosamples with a cauliflower-like morphology. The particles displayed irregular shapes with multiple protrusions resembling the florets of a cauliflower. The surface appeared more textured compared to the samples annealed at lower temperatures. The average particle size was measured to be approximately 23 nm, indicating a slight increase in size compared to the samples annealed at lower temperatures.

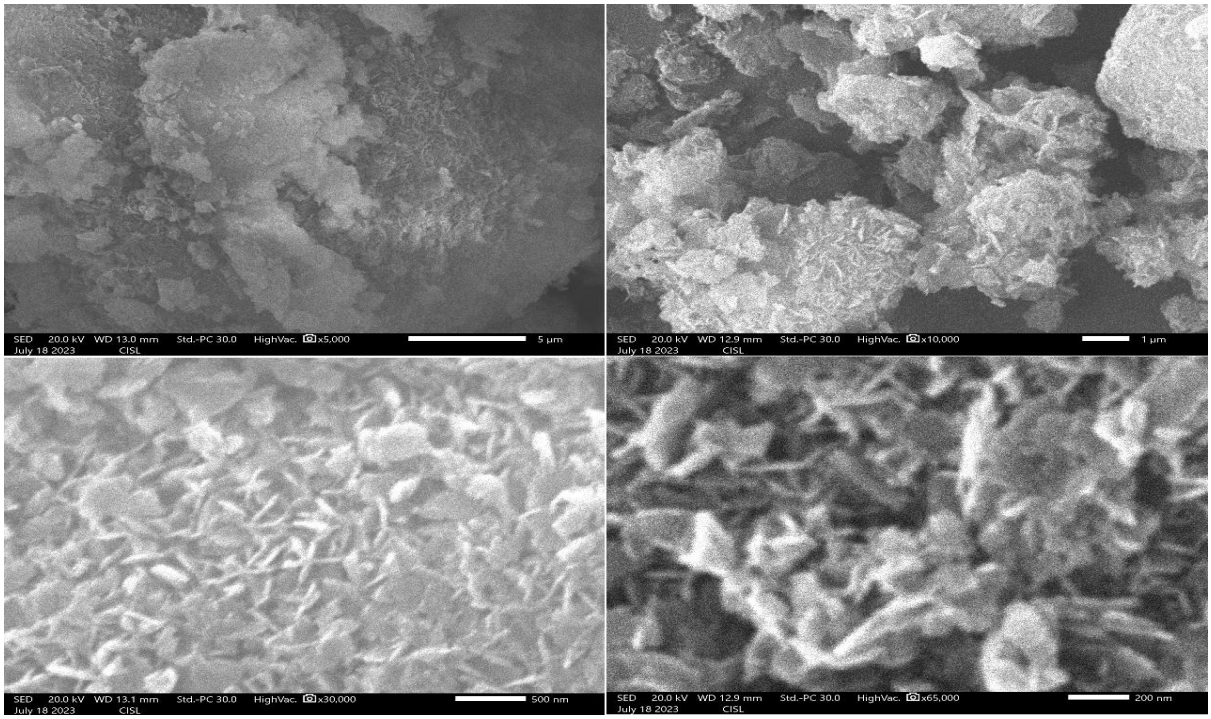

Figure 6 (a): SEM micrographs of Diarun 50% + MgO 50% nanosamples for magnification at 200℃

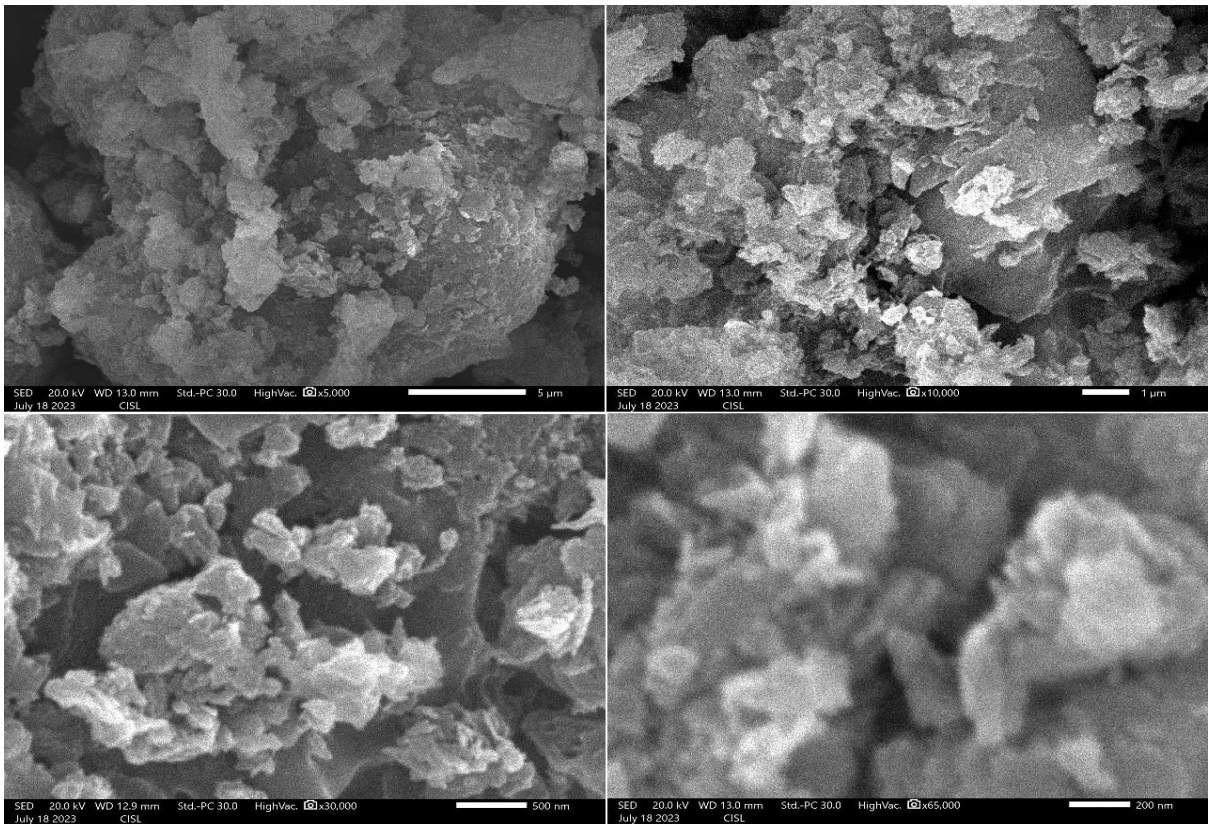

Figure 6 (b): SEM micrographs of Diarun 50% + MgO 50% nanosamples for magnification at 400℃

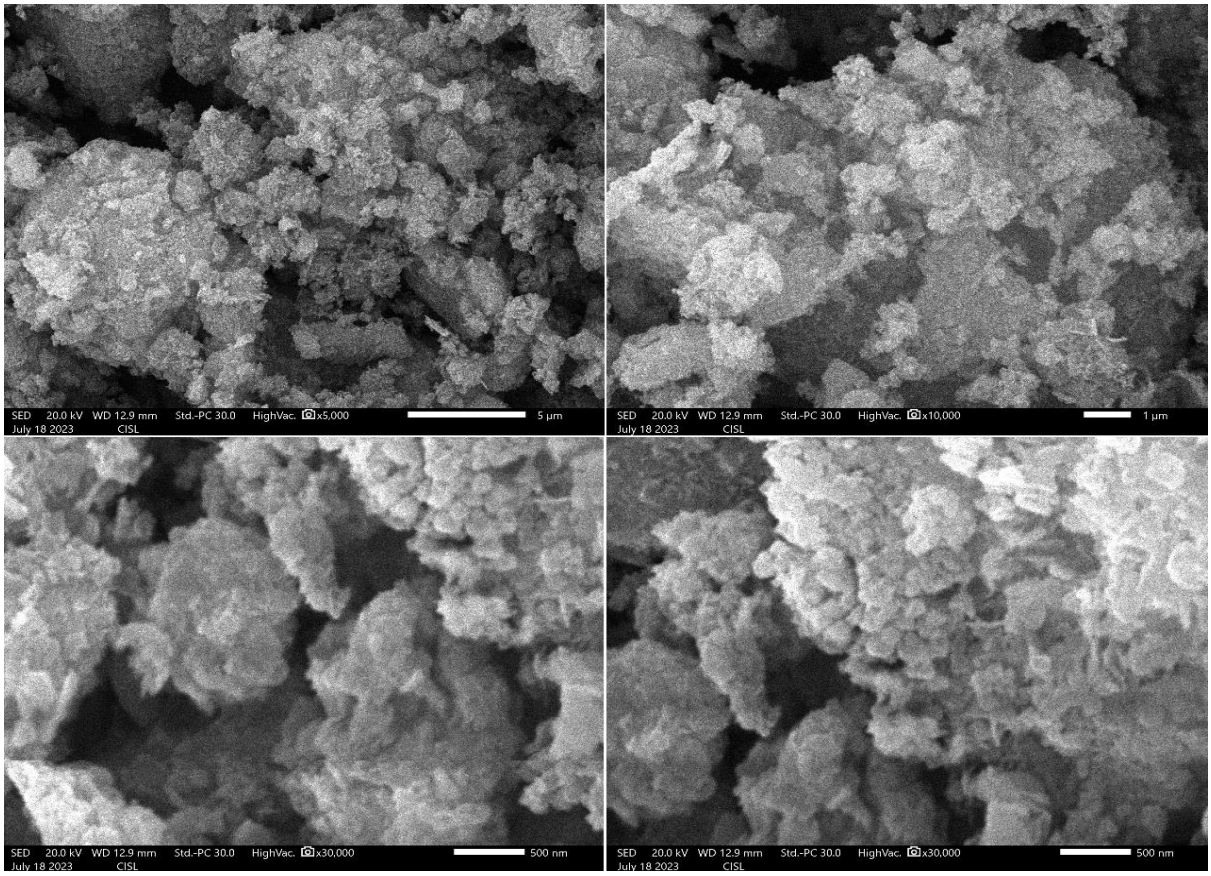

Figure 6 (c): SEM micrographs of Diarun 50% + MgO 50% nanosamples for magnification at 600℃

3.5. Atomic Force Microscope Analysis

AFM images of Diarun (50%) + MgO (50%) nanoparticles obtained at different annealing temperatures revealed distinct variations in the surface morphology of the nanoparticles. Analyzing the nanocomposites in both vertical and horizontal orientations enabled the identification of any directional variations in grain size. The flatness profile along vertical and horizontal lines demonstrated the uniformity of the nanoparticle surfaces shown in figure (a, b, d, e, g, h) at different annealing temperature. The histogram distribution of grain size provided a statistical representation of the grain size distribution within the nanoparticle. Furthermore, the 3D view of surface roughness shown in figure (c, f, i). This approach allowed for quantitative assessments, encompassing parameters such as root mean square roughness (Rq) and average roughness (Ra) and grain size measurements are listed in table 3, in addition to comprehensive scrutiny of images from different perspectives. The grain size analysis showed a decrease in grain size with increasing annealing temperature, with values of 14.825 nm at 200°C, 9.11 nm at 400°C, and 11.065 nm at 600°C.

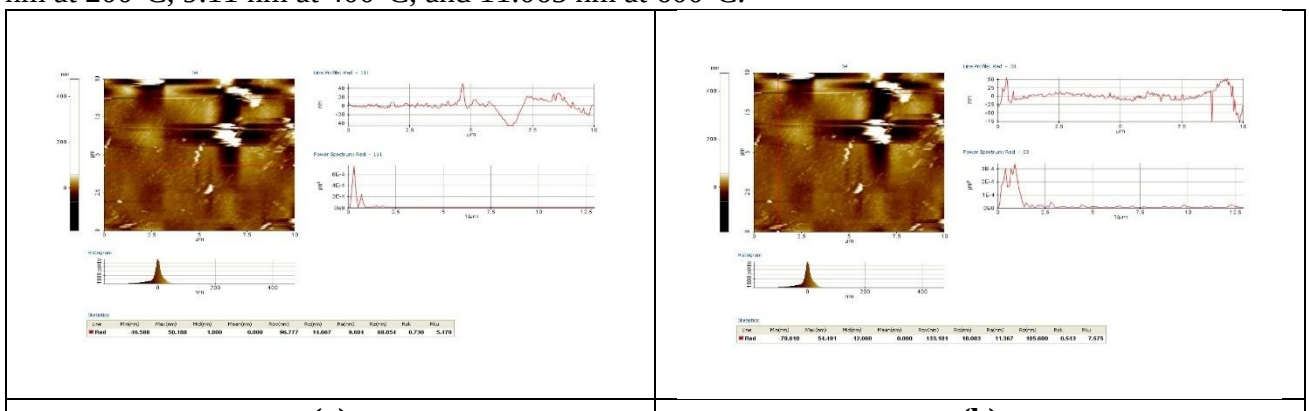

(a) **(b)**

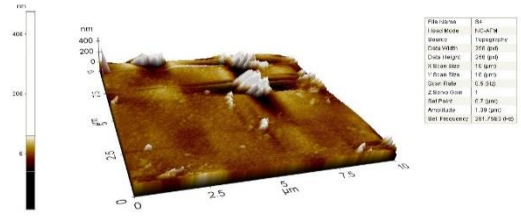

(c)

Figure 7 (a-c): AFM images of the Diarun (50%) + MgO (50%) nanoparticles at 200°C (a, b) flatness profile (vertical and horizontal line) and histogram distribution of grain size, (c) 3D view of surface roughness

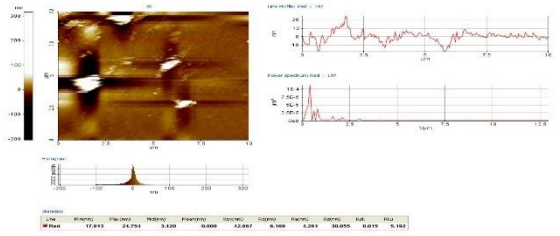

(d)

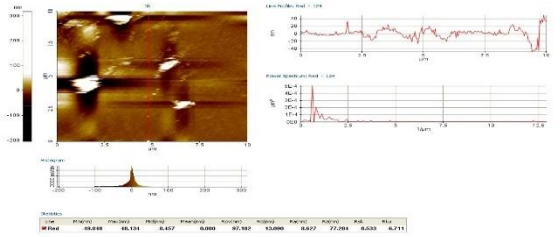

(e)

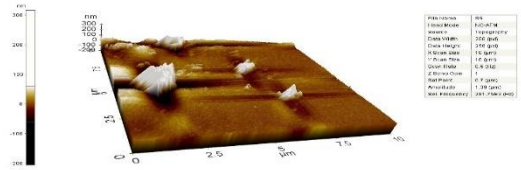

(f)

Figure 7 (d-f): AFM images of the Diarun (50%) + MgO (50%) nanoparticles at 400°C (d, e) flatness profile (vertical and horizontal line) and histogram distribution of grain size, (f) 3D view of surface roughness

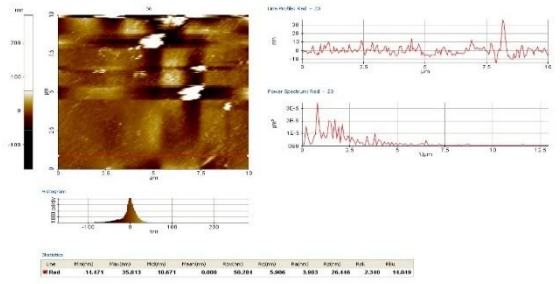

(g)

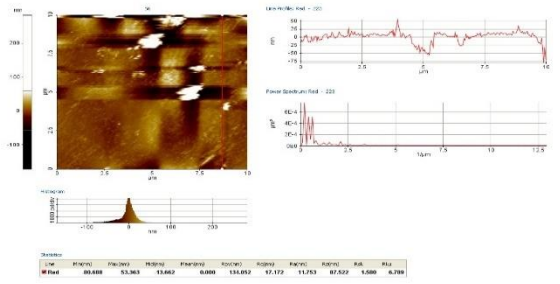

(h)

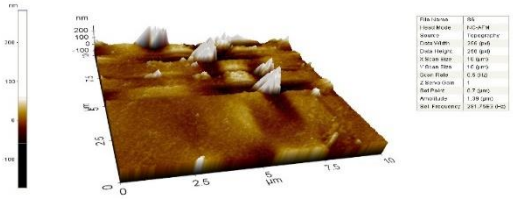

(i)

Figure 7 (g-i): AFM images of the Diarun (50%) + MgO (50%) nanoparticles at 600°C (g, h) flatness profile (vertical and horizontal line) and histogram distribution of grain size, (i) 3D view of surface roughness

Table 3: Surface characteristics and grain size of Diarun (50%) + MgO (50%) at different annealed temperature

Annealing Temperature (°C)		Rq (nm)	Ra (nm)	Grain Size (nm)
200	V	18.083	11.367	16.07
	H	14.667	9.604	13.58
400	V	13.090	8.627	12.2
	H	6.169	4.261	6.02
600	V	17.172	11.753	16.62
	H	5.906	3.903	5.51

3.6. Particle Size Analyser

To investigate the effect of annealing temperatures on the particle size distribution of Diarun 50% + MgO 50% nanocomposites, a particle size analyzer was employed and shown in figure 8. The particle size distribution of the nanocomposites exhibited a decrease in the average particle size with increasing annealing temperature. This trend is consistent with the thermal decomposition and sintering of the nanocomposites, which leads to the formation of smaller and more uniform particles. The polydispersity index, which indicates the degree of particle size distribution, also decreased with increasing annealing temperature, suggesting a more uniform particle size distribution at higher temperatures.

The results indicate that the annealing process at 600°C produced the smallest average particle size (D(50%) = 136.2 nm) and the most uniform particle size distribution (polydispersity index = 0.296). This suggests that the nanocomposites synthesized at 600°C have the potential to exhibit enhanced thermal properties due to the smaller and more uniform particle size distribution. In contrast, the annealing process at 200°C produced the largest average particle size (D(50%) = 140.2 nm) and the least uniform particle size distribution (polydispersity index = 0.285). This indicates that the nanocomposites synthesized at 200°C may have inferior thermal properties due to the larger and more heterogeneous particle size distribution. The annealing process at 400°C produced an intermediate particle size distribution (D(50%) = 117.7 nm) and polydispersity index (0.315), suggesting that the nanocomposites synthesized at 400°C may have a balance between thermal properties and particle size distribution.

In summary, the particle size analysis of Diarun-MgO nanocomposites revealed that the annealing process at 600°C produced the smallest and most uniform particle size distribution, which may lead to enhanced thermal properties. The annealing process at 200°C produced the largest and least uniform particle size distribution, which may lead to inferior thermal properties. The annealing process at 400°C produced an intermediate particle size distribution, which may lead to a balance between thermal properties and particle size distribution. These findings provide valuable insights into the optimization of Diarun-MgO nanocomposites for various thermal management applications.

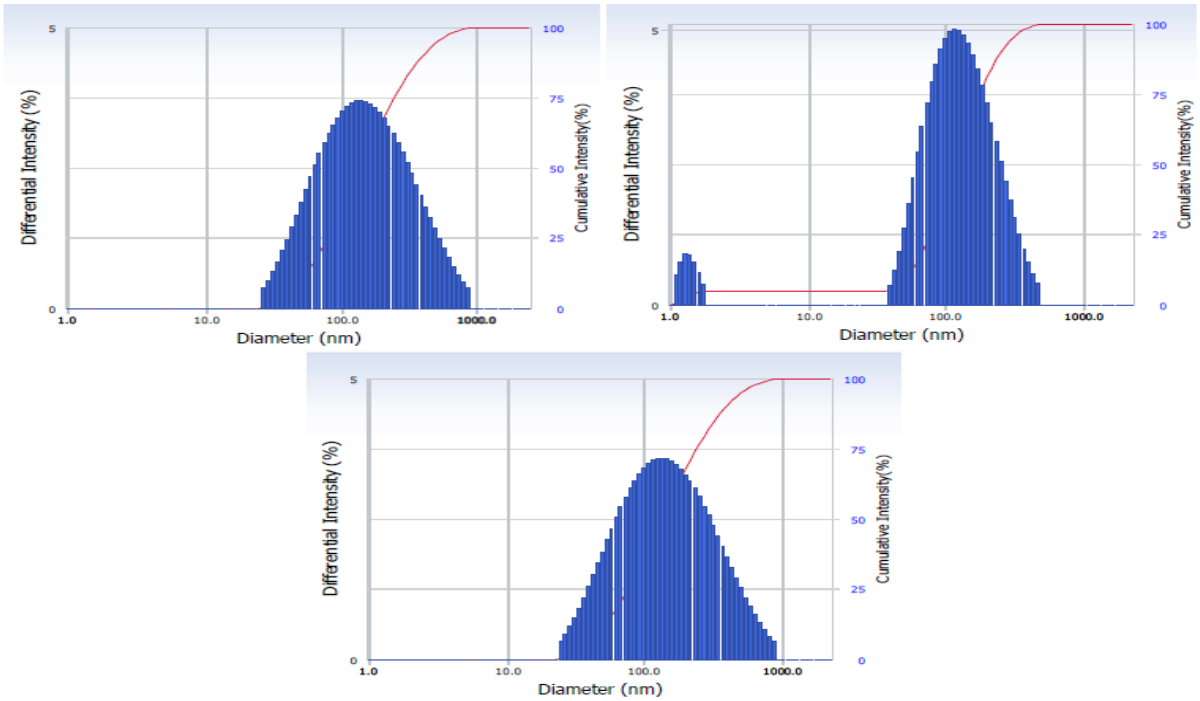

Figure 8: Particle size distribution of Diarun 50% + MgO 50% nanocomposites at annealing temperatures of 200°C, 400°C, and 600°C

3.7. Conclusion

In conclusion, the comprehensive investigation of Diarun 50% + MgO 50% nanocomposites synthesized via wet chemical methods and subjected to varying annealing temperatures has provided valuable insights into their structural evolution and properties. Through a combination of analytical techniques including X-ray diffraction (XRD), Fourier-transform infrared (FTIR) spectroscopy, Williamson-Hall analysis, and dislocation density measurements, a detailed understanding of the nanocomposites' characteristics has been achieved. The XRD analysis revealed distinct diffraction peaks corresponding to different crystallographic planes at each annealing temperature, indicating variations in crystallinity. Furthermore, the determination of average crystallite sizes using the Debye's-Scherrer equation demonstrated a clear temperature-dependent effect on crystallite growth. These findings underscore the significance of annealing conditions in modulating the structural characteristics of nanocomposite materials. FTIR spectroscopy provided insights into chemical bonding and functional group changes, while SEM imaging revealed morphological variations. Particle size analysis elucidated size distribution trends, and AFM imaging captured surface topography alterations. Moving forward, optimizing synthesis parameters and annealing protocols will be essential for tailoring the structural and functional properties of Diarun-MgO nanocomposites to meet specific application requirements. Overall, this study contributes to a deeper understanding of the relationship between synthesis conditions, annealing processes, and the resulting properties of nanocomposite materials, laying the foundation for their utilization in various technological applications.

References:

[1]Nel, A., Xia, T., Mädler, L., & Li, N. (2006). Toxic potential of materials at the nano level. Science, 311(5761), 622-627.

[2]Yin, Y., Alivisatos, A. P., & Gates, B. D. (2002). Synthesis and characterization of stable colloidal cobalt nanoparticles. Journal of the American Chemical Society, 124(46), 13642-13643.

[3]K. Krishnamoorthy, J.Y. Moon, H.B. Hyun, S.K. Cho, S.J. Kim, J. Mater. Chem. 22 (2012) 24610e24617.

[4]M. Deepa, A.K. Srivastava, S.A. Agnihotry, Acta Mater. 54 (2006) 4583e4595.

[5]Kumari, S., &Panghal, M. (2020). Herbal extracts as potential dopants for metal oxide nanoparticles: A review. Materials Today: Proceedings, 26, 2779-2784.

[6]N.A. Richter, S. Sicolo, S.V. Levchenko, J. Sauer, M. Scheffler, Phys. Rev. Lett. 111(2013) 045502.

[7]A. Chanthbouala, R. Matsumoto, J. Grollier, V. Cros, A. Anane, A. Fert, A.V. Khvalkovskiy, K.A. Zvezdin, K. Nishimura, Y. Nagamine, H. Maehara,K. Tsunekawa, A. Fukushima, S. Yuasa, Nat. Phys. 7 (2011) 626e630.
[8]Li, Y., Zhou, Y., Wang, H., Sun, Q., & Zhou, Y. (2020). Recent advances in the synthesis, properties, and applications of magnesium oxide nanoparticles: A review. Ceramics International, 46(16), 25181-25202.
[9]Singh, A. K., & Bhatnagar, A. (2020). A review on synthesis and properties of magnesium oxide (MgO) nanoparticles. Materials Today: Proceedings, 23, 1443-1446.
[10] Li, S., Liu, H., Xie, Z., Yu, W., & Zhang, Y. (2017). Hydrothermal synthesis of magnesium oxide nanoparticles for photocatalytic degradation of acetylsalicylic acid. Materials Letters, 209, 527-529.
[11] Kumar, V., Sharma, N., Nayan, R., & Singh, R. K. (2017). A Review on Synthesis and Characterization of Nano Magnesium Oxide by Solution Combustion Method. International Journal of Advanced Research in Science, Engineering and Technology, 4(5), 4378-4383.
[12] Lina, A., Mahmooda, A., Mansourb, S. A., &Zedana, A. F. (2019). Synthesis of magnesium oxide nanoparticles via chemical precipitation method for photo-degradation of Rhodamine B dye. Journal of Molecular Liquids, 285, 471-480.
[13] Tran, H. N., Hwang, H. M., & Nguyen, T. D. (2019). Synthesis and applications of magnesium oxide nanoparticles: A review. Chemosphere, 232, 552-567.
[14] Y. Lin, A. B€oker, J. He, K. Sill, H. Xiang, C. Abetz, X. Li, J. Wang, T. Emrick, S.Long, Q. Wang, A. Balazs, T.P. Russell, Nature 434 (2005) 55e59.
[15] J. Goniakowski, C. Noguera, L. Giordano, Phys. Rev. Lett. 93 (2004) 215702.
[16] A.S. Aric_o, P. Bruce, B. Scrosati, J.M. Tarascon, W.V. Schalkwijk, Nat.Mater. 4 (2005)366e377.
[17] Y.G. Zhang, H.Y. He, B.C. Pan, J. Phys. Chem. C 116 (2012) 23130e23135.
[18] K. Zhu, W. Hua, W. Deng, R.M. Richards, Eur. J. Inorg. Chem. 2012 (2012) 2869e2876.
[19] L. Qina, J. Zhaob, X. Zou, Mater. Chem. Phys. 113 (2009) 468e473.
[20] X.Y. Yu, T. Luo, Y. Jia, Y.X. Zhang, J.H. Liu, X.J. Huang, J. Phys. Chem. C 115 (2011) 22242e22250.
[21] K. Karthikeyan, S. Amaresh, V. Aravindana, Y.S. Lee, J. Mater. Chem. A 1 (2013) 4105e4111.
[22] Y. Qu, W. Zhou, Z. Ren, K. Pan, C. Tian, Y. Liu, S. Feng, Y. Dong, H. Fu, Eur. J.Inorg. Chem. 2012 (2012) 954e960.
[23] M. Haertelt, A. Fielicke, G. Meijer, K. Kwapien, M. Sierkaz, J. Sauer, Phys. Chem.Chem. Phys. 14 (2012) 2849e2856.
[24] Z. Li, C.V. Ciobanu, J. Hu, J.P.P. B_aez, J.L.R. L_opezd, R. Richards, Phys. Chem.Chem. Phys. 13 (2011) 2582e2589.
[25] E.H.H. Chow, F.C. Strobridge, T. Fri_s_ci_c, Chem. Commun. 46 (2010) 6368e6370.
[26] L. Yan, J. Zhuang, X. Sun, Z. Den, Y. Li, Mater. Chem. Phys. 76 (2002) 119e122.